9255

Theoretical Study on the Singlet Excited State of Pterin and Its Deactivation Pathway[†]

Xing Chen, Xuefei Xu, and Zexing Cao*

Department of Chemistry and State Key Laboratory of Physical Chemistry of Solid Surfaces,
Xiamen University, Xiamen 361005, China

Received: April 9, 2007; In Final Form: May 21, 2007

The excited-state properties and related photophysical processes of the acidic and basic forms of pterin have been investigated by the density functional theory and ab initio methodologies. The solvent effects on the low-lying states have been estimated by the polarized continuum model and combined QM/MM calculations. Calculations reveal that the observed two strong absorptions arise from the strong $\pi \rightarrow \pi^*$ transitions to $^1(\pi\pi^*L_a)$ and $^1(\pi\pi^*L_b)$ in the acidic and basic forms of pterin. The first $^1(\pi\pi^*L_a)$ excited state is exclusively responsible for the experimental emission band. The vertical $^1(n_N\pi^*)$ state with a small oscillator strength, slightly higher in energy than the $^1(\pi\pi^*L_a)$ state, is less accessible by the direct electronic transition. The $^1(n_N\pi^*)$ state may be involved in the photophysical process of the excited pterin via the $^1(\pi\pi^*L_a/n_N\pi^*)$ conical intersection. The radiationless decay of the excited PT to the ground state experiences a barrier of 13.8 kcal/mol for the acidic form to reach the (S_1/S_0) conical intersection. Such internal conversion can be enhanced with the increase in excitation energy, which will reduce the fluorescence intensity as observed experimentally.

1. Introduction

Pterins (PTs) and their derivatives are the important members of heterocyclic compounds that are widespread in biological systems. They participate in relevant biological functions, behaving as inhibitors,[1] enzymes,[2−4] coenzymes,[5,6] sensitizers,[7,8] and pigments.[9] For example, tetrahyrobiopterin as a coenzyme was involved in the metabolism of some amino acids and nitric oxides. Because of their high biological relevance, the determination of the concentration of pterins in body fluids also has been used for clinical purposes.[10]

Since the sensitivity of pterins to light was observed half a century ago,[11] these heterocyclic compounds have had a standing interest in photophysics and photochemistry.[12,13] The development and wide application of fluorescence analytical techniques also stimulate the study of photophysical and photochemical properties of PTs. The fluorescence emission from PTs has been used for analysis of their concentration and exploration of interactions of nucleic acids with proteins. Recently, some pteridine-based fluorophores as chemical analogues of the DNA nucleosides have been established in the study of the physicochemical properties of DNA.[14−16]

In the past decade, the excited-state properties of PTs have been systematically studied.[17−23] More recently, Lorente and Thomas reported their experimental study on the photochemistry and photophysics of PTs in aqueous solution. From an experimental point of view, they assigned the absorption and emission spectra of PTs and proposed plausible decay mechanism of excited PTs. Under UV-A irradiation, the excited PTs may undergo photooxidation besides fluorescence emission. The reactive oxygen species can be generated as the photoproduct, such as the singlet molecular oxygen ($^1O_2$), which is one of the main reactive species responsible for the light-induced damage of biological systems. Such fascinating photochemical properties of PTs were found to depend on both the chemical structure and the pH of environments. Despite their important contribution, the electronic and geometrical features of related low-lying states as well as the explicit mechanism of photochemistry and photophysics of PTs are still unclear.

In the present work, we performed extensively theoretical calculations on the acidic and basic forms of PT in their ground and excited states. Their strong absorption (250−360 nm) and emission (∼450 nm) in aqueous solution have been interpreted on the basis of sophisticated ab initio calculations. Possible radiationless decay channels of the excited PT have been discussed.

2. Computational Details

Geometry optimizations and vibrational analyses of the acid and basic forms of pterin in the gas phase have been performed by the B3LYP functional.[24] In the calculation, different basis sets, including the 6-311G** for the acidic form and the 6-31++G** for the basic form, have been used. In consideration of the solvent effect, the equilibrium geometries of acid and basic forms of PT in aqueous solution have been optimized by the B3LYP approach in connection to the polarized continuum model (PCM)[25] with the 6-311G* and 6-31+G* basis sets, respectively. These calculations were carried out with the Gaussian 03 program package.[26]

We also performed combined QM/MM calculations to explore the ground-state geometries of PT in aqueous solution. The QM/MM model was built by solvating the PT molecule in a water sphere of 10 Å radius, followed by 10ps molecular dynamics (MD) simulations with CHARMM22[27] to bring the system to an equilibrium. The spherical model of the acid form contains 419 atoms, including pterin and 134 water molecules. For the basic form of PT, a sodium cation is introduced into the model to balance the total charges. In the QM/MM calculation, the QM region consists of PT and the water molecules, which have relatively strong hydrogen bond interactions with PT. The B3LYP functional and the 6-31G* basis set were used for the QM part in the QM/MM treatment, and the

MM part was described by the CHARMM22 force field. The ChemShell package[28] integrating TURBOMOLE[29] was employed in the QM/MM calculation.

The vertical transition energies of the low-lying excited states of PT have been calculated by the time-dependent density functional theory (TD-B3LYP)[30] at the optimized ground-state structures under different conditions. For comparison, the vertical transition energies in the gas phase have been estimated by the multiconfiguration second-order perturbation theory (CASPT2) method incorporating the dynamic correlation effects. A level-shift technique with an imaginary shift of 0.3 au was applied in order to moderate the effect of intruder states in the CASPT2 calculation.

The search for local minima, conical intersections, and saddle points on the excited-state potential energy surfaces of PT were performed with the CASSCF[31] approach implemented in the Gaussian 03 program package. The active spaces used in the CASSCF computation were mainly composed of low-energy frontier π orbitals and two lone pair orbitals, which were important for description of the molecular nature of PT. In the geometry optimization of the acid form of PT in the excited state, the active space includes 12 electrons distributed over nine low-energy valence orbitals, denoted as CAS(12, 9). For the basic form, the CAS(12, 10) active space was employed. The 6-311G* and 6-31G** basis sets were used in the CASSCF calculation for the acidic and basic forms, respectively.

In the location of the conical-intersection and saddle-point geometries, the active space in the CASSCF calculation has been reduced to CAS(8,6) and CAS(8,7) for the acidic and basic forms, respectively, considering the computational costs and avoiding the intrusion of outer states. Test calculations indicate that use of relatively small active space was still adequately for geometry optimization. The initial geometry of the saddle point connecting a given conical intersection and a given local minimum on the excited-state potential energy surface was obtained by constructing a linearly interpolated internal-coordinate (LIIC) reaction path. The LIIC reaction path was defined as the straight line in the multidimensional internal-coordinate space connecting two given structures. The LIIC strategy provides a qualitative overview of the diabatic state correlations, although it does not give quantitative energetic information. The single-point energies on the LIIC path were calculated at the CAS(12,9)/6-311G* and CAS(12,10)/6-31G** levels for the acidic and basic forms with the MOLPRO 2006 program,[32] respectively. After the key points on the potential energy surfaces of the low-lying states were located, their relative energies were reevaluated by CASPT2.

3. Results and Discussions

3.1. Ground-State Geometries. The equilibrium geometries of the acidic and basic forms of PT at the ground state in the gas phase and in aqueous solution have been determined by different methods. The acidic form of PT has four tautomers in its ground state,[33] but only the most stable species was considered here. Figure 1 displays the optimized structures of the lowest-energy acidic and basic forms by B3LYP, B3LYP-PCM, and QM/MM calculations.

As Figure 1 displays, the acid form has a near planar structure in the gas phase (**1**). In aqueous solution, the acidic form exhibits an elongated carbonyl group (**2** and **3**) and C−NH₂ bond in comparison with the gas-phase structure. In particular, the QM/MM-optimized geometry (**3**) showed a pyramidized amino group in solution, where the C═O bond length is 1.243 Å, longer than the 1.208 Å length in the gas phase. Such
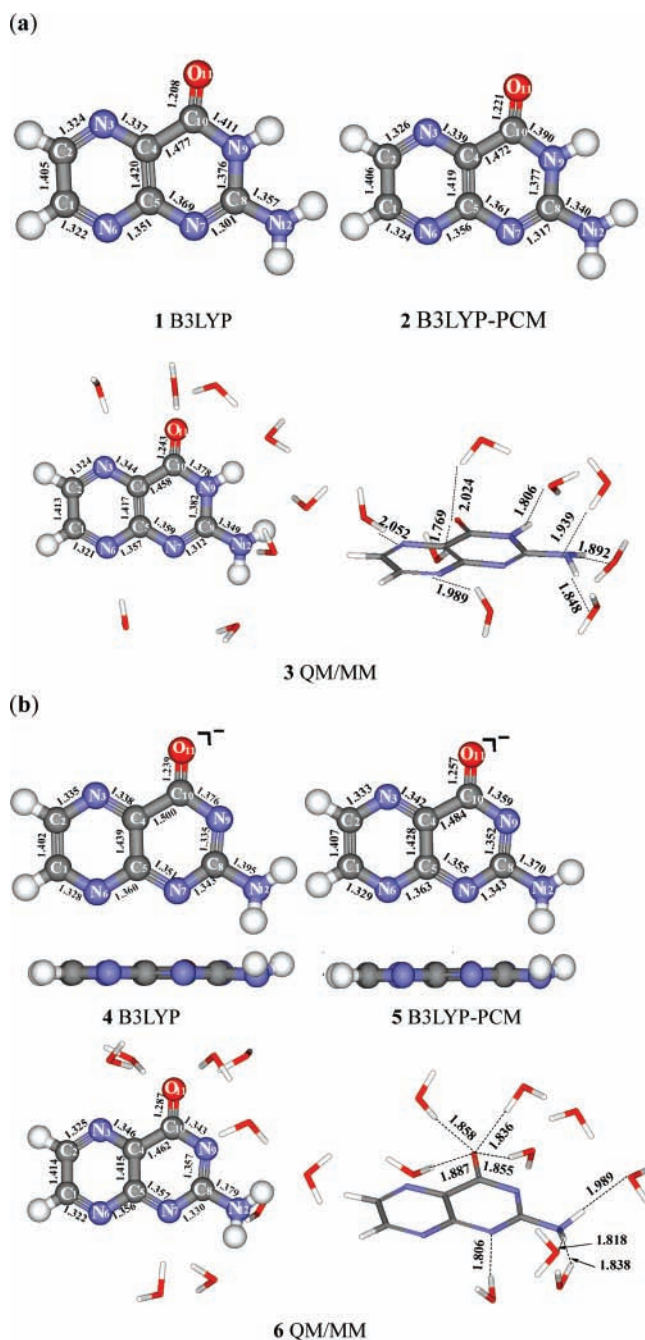

Figure 1. Optimized ground-state geometries (distances in angstroms and angles in degrees) of the acidic form (a) and the basic form (b) of pterin in the gas phase and in solution by B3LYP and QM/MM (QM = B3LYP; MM = CHARMM).

geometrical features can be ascribed to hydrogen-bond interactions between water molecules and PT, as shown in Figure 1.

For the basic form, the equilibrium geometries both in the gas phase (**4**) and in aqueous solution (**5** and **6**) exhibit a slightly pyramidized amino group. Like the acidic form, in aqueous solution, the C₁₀−O₁₁ and C₈−N₁₂ bond lengths increase relative to those of the gas-phase structure. The presence of the solvent water enhances the distortion of the amino group. The B3LYP calculations predict that the neutral acid form and the anionic basic form have dipole moment of 4.47 and 4.39 Debye in the gas phase, respectively.

3.2. Vertical Excitations. Properties of the interested low-lying singlet excited states in both acid and basic forms have been studied by different theoretical methods. Predicted vertical excitation energies, oscillator strengths, and dipole moments,

Singlet Excited State of Pterin and Its Deactivation Pathway

J. Phys. Chem. A, Vol. 111, No. 38, 2007 **9257**

TABLE 1: Vertical Transition Energies (in eV) of Low-Lying Singlet Excited States of the Acidic Form and Basic Form of Pterin by Different Approaches

| | gas phase | | aqueous solution | | |
state	CASPT2[a]	TD-B3LYP	TD-B3LYP	TD-QM/MM	exp.[b]
		acidic form			
$^1(\pi\pi^*L_a)$	3.984(0.1783)[3.425]	3.950(0.0908)	3.694(0.1224)	3.756(0.1058)	3.65
$^1(n_N\pi^*)$	4.015(0.0066)[0.659]	3.151(0.0019)	3.619(0.0023)	3.601(0.0014)	
$^1(n_O\pi^*)$	4.714(0.0016)[0.241]	4.430(0.0001)	4.501(0.0000)	4.458(0.0014)	
$^1(\pi\pi^*L_b)$	5.800(0.1423)[2.544]	4.831(0.2103)	4.750(0.2487)	4.778(0.1781)	4.59
		basic form			
$^1(\pi\pi^*L_a)$	3.228(0.1166)[3.085]	3.407(0.0702)	3.527(0.1246)	3.891(0.1262)	3.46
$^1(n_N\pi^*)$	3.563(0.0003)[0.137]	3.123(0.0006)	3.420(0.0011)	3.537(0.0017)	
$^1(\pi\pi^*L_b)$	4.123(0.0798)[2.759]	4.638(0.2564)	4.796(0.3432)	5.207(0.3012)	4.92

[a] Oscillator strengths are in parentheses, and dipole moments (in Debye) are in brackets by CASSCF. [b] See ref 23.

TABLE 2: Predicted and Experimental Emission Energies (F, eV) and Lifetime (τ_{rad}, ns) of Low-Lying Singlet Excited States of the Acidic Form and Basic Form of Pterin

state	theory[a]	exp.[b]
	acidic form	
$^1(\pi\pi^*L_a)_{min}$	3.14 (2.66)	2.82 (22)
$^1(n_N\pi^*)_{min}$	3.36 (0.26)	
$^1(n_O\pi^*)_{min}$	3.42 (4.25)	
	basic form	
$^1(\pi\pi^*L_a)_{min}$	2.61 (0.94)	2.72 (18)

[a] Lifetimes are in parentheses. [b] See ref 23, where $\tau_{rad} = \tau_F/\Phi_F$; for the acidic form, $\Phi_F = 0.33 \pm 0.01$, $\tau_F = 7.6$ ns; for the basic form, $\Phi_F = 0.27 \pm 0.01$, $\tau_F = 5.0$ ns.

as well as the character of the electronic excitations, are presented in Table 1. For comparison, available experimental values are incorporated into Table 1.

All calculations show that all electronic transitions to the $^1(\pi\pi^*)$ states have large oscillator strengths and that they correspond to the strong absorptions observed in experiment. On the contrary, the electronic excitations from the ground state to $^1(n\pi^*)$ states have relatively small oscillator strengths less than 0.01, and thus direct transitions to these $^1(n\pi^*)$ states are difficult to characterize experimentally, especially when they overlap with strong $\pi \rightarrow \pi^*$ transitions. Because of the inaccessibility of the $^1(n\pi^*)$ state, the reliable experimental data for the $^1(n\pi^*)$ state is scarce. However, the $^1(n\pi^*)$ state is usually vitally important for the ultrafast internal conversion (IC) processes to the ground state.[34]

CASPT2 calculations at the B3LYP-optimized geometries of the ground state indicate that in the gas phase, the lowest excited states of both the acidic and basic forms are ($^1\pi\pi^*L_a$) states, derived mainly from one-electron promotion from the highest occupied molecular orbital (HOMO) to the lowest unoccupied molecular orbital (LUMO). The $^1(n_N\pi^*)$ states are characterized by one electronic excitation from one N lone pair orbital in molecular plane to a π antibonding orbital. The $^1(n_N\pi^*)$ state of the acidic form of PT is slightly higher in energy than the ($^1\pi\pi^*L_a$) state by ~0.03 eV, but the energy splitting between the $^1(n_N\pi^*)$ and ($^1\pi\pi^*L_a$) states increases to 0.3 eV in the basic form. For both forms, higher-lying $^1(\pi\pi^*)$ states were identified as ^1L_b,[35] which basically arise from the HOMO $\rightarrow$ LUMO + 1 and HOMO-1 $\rightarrow$ LUMO transitions.

It should be noted that the energy order of the two lowest-lying excited singlet states depends on the use of methodology, and CASPT2//B3LYP calculations predict that the ($^1\pi\pi^*L_a$) state is the first excited state, whereas the $^1(n_N\pi^*)$ state is the lowest excited-state by TD-B3LYP//B3LYP (Table 1).

As shown in Table 1, the calculated dipole moments of the low-lying excited states are evidently different from those of

the ground states, except the $^1(\pi\pi^*L_a)$ states. Thus, the solvent effect on the low-lying states may be remarkable in polar aqueous solution. TD-B3LYP with the PCM model and condensed-phase QM/MM calculations have been employed to determine the absorption spectra of PT in aqueous solution. Inspection of the data in Table 1 reveals that predicted transition energies by both TD-B3LYP and QM/MM agree with the experimental observation. Especially the TD-B3LYP calculations with the PCM model give excitation energies with an accuracy of no more than 0.15 eV. The calculations show that the strong absorptions of the acidic and basic forms in aqueous solution occur at 4.75 and 4.80 eV, respectively, which can match the experimental bands centered at 4.59 eV (270 nm) and 4.92 eV (252 nm).[23] The red-shifted transition in the acidic form is relatively weak in comparison with the corresponding peak in the basic form. Other strong absorptions in the acidic and basic forms occur at 3.69 and 3.53 eV, respectively. Both transitions have comparable oscillator strengths, whereas the $\pi \rightarrow \pi^*$ transition in the acid form exhibits a blue-shifted character related to that in the basic form.

The present TD-B3LYP calculations suggest that in aqueous solution, the $^1(n_N\pi^*)$ absorptions are blue-shifted as compared with those in the gas phase, which leads to the close-lying $^1(\pi\pi^*L_a)$ and $^1(n_N\pi^*)$ states. Therefore, the $^1(n\pi^*)$ state may be involved in the deactivation processes back to the ground state via conical intersection caused by the strong vibronic interaction between $^1(\pi\pi^*L_a)$ and $^1(n_N\pi^*)$,[34] though the $^1(n_N\pi^*)$ state is difficult to directly populate because of its relatively small oscillator strength with respect to the $^1(\pi\pi^*)$ state.

3.3. Key Structures on the Excited-State Potential Energy Surfaces. *Acidic Form of PT.* Equilibrium geometries of excited states $^1(\pi\pi^*L_a)_{min}$, $^1(n_N\pi^*)_{min}$, and $^1(n_O\pi^*)_{min}$ on the potential energy surfaces of the acidic form of PT have been determined by CASSCF. Figure 2 displays the CASSCF-optimized structures of these low-lying states. Like the ground state, these excited states have optimized planar structures. The $^1(\pi\pi^*L_a)_{min}$ state (**7**) has elongated C_1N_6, N_7C_8 and C_9C_{10} bonds related to the ground state, as a result of the HOMO (π) $\rightarrow$ LUMO (π^*) transition. The pyrazine ring in the $^1(n_N\pi^*)_{min}$ structure (**8**) is significantly deformed, where the angle of $A(C_2N_3C_4)$ increases from 116.5° in the ground-state geometry to 126.9° because of the involvement of electronic excitation from the in-plane long-pair orbital of N_3.

In the ground state, the N_3 atom adopts a sp² hybridization, and strong repulsion interactions of in-plane N_3 lone pair electrons with C_2N_3 and N_3C_4 bonds lead to a small bond angle of $A(C_2N_3C_4)$. With the electronic transition from the in-plane N_3 lone pair orbital to the perpendicular π^* orbital, the repulsion interactions decrease and give rise to the relaxation of $A(C_2N_3C_4)$. However, no out-of-plane distortion has been found in the
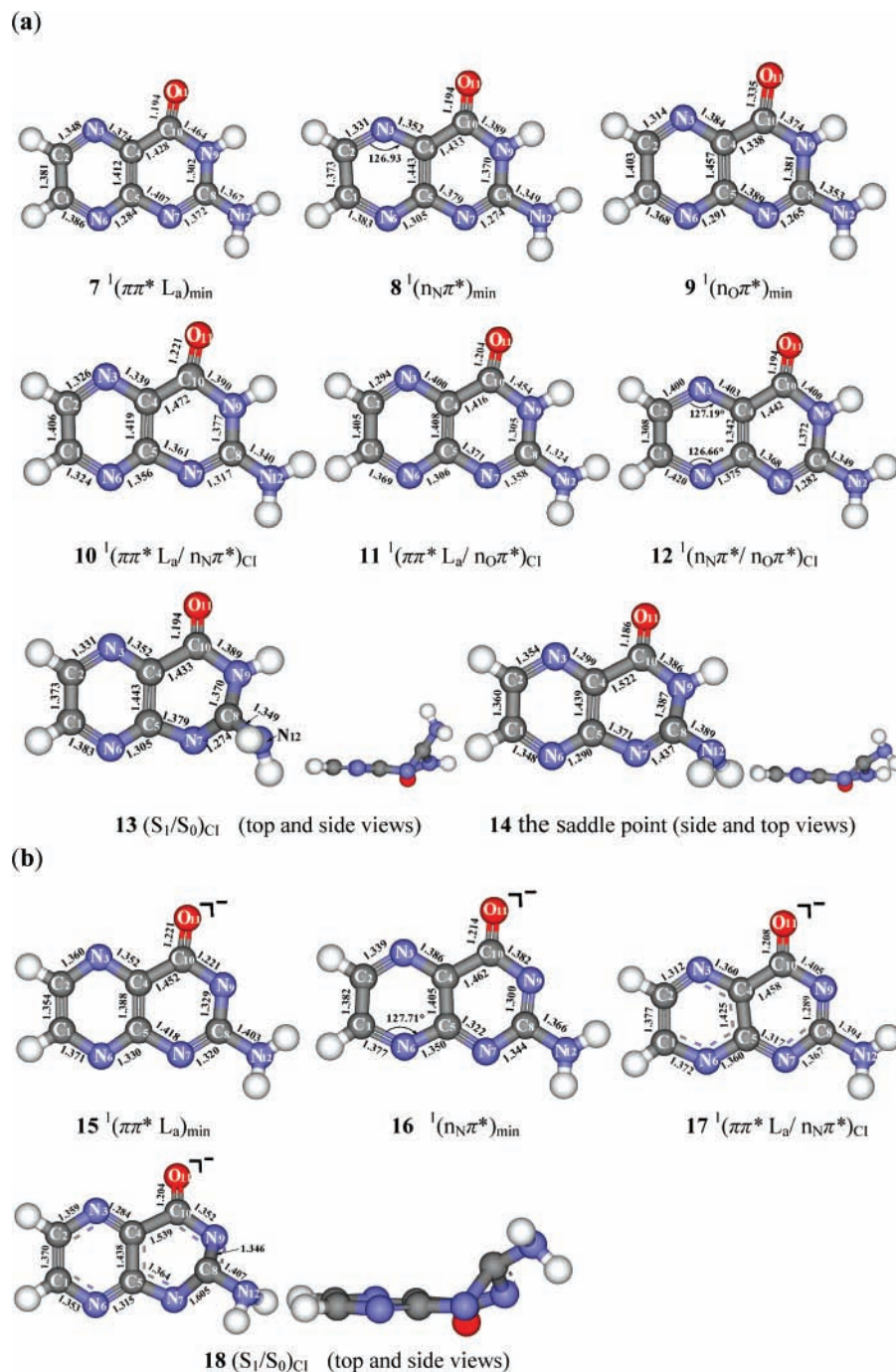
(a)

7 $^1(\pi\pi^* L_a)_{min}$ 8 $^1(n_N\pi^*)_{min}$ 9 $^1(n_O\pi^*)_{min}$

10 $^1(\pi\pi^* L_a/ n_N\pi^*)_{CI}$ 11 $^1(\pi\pi^* L_a/ n_O\pi^*)_{CI}$ 12 $^1(n_N\pi^*/ n_O\pi^*)_{CI}$

13 $(S_1/S_0)_{CI}$ (top and side views)   14 the saddle point (side and top views)

(b)

15 $^1(\pi\pi^* L_a)_{min}$ 16 $^1(n_N\pi^*)_{min}$ 17 $^1(\pi\pi^* L_a/ n_N\pi^*)_{CI}$

18 $(S_1/S_0)_{CI}$ (top and side views)

Figure 2. 2. CASSCF-optimized geometries (distances in angstroms and angles in degrees) of the acidic form (a) and the basic form (b) of pterin in their excited states, conical intersections, and saddle points.

present optimized $^1(n_N\pi^*)_{min}$ structure. This is different from the $^1(n\pi^*)$ equilibrium geometry of 9H-adenine where there is an out-of-plane distortion arising from vibronic coupling of the $^1(n\pi^*)$ state with the $^1(\pi\pi^*)$ state via out-of-plane coupling modes.[36–39] A possible explanation is that there is a stronger π-electron conjugation in PT with two six-membered rings. The remarkably elongated carbonylic bond of 1.34 Å is the most evidently geometrical feature of the $^1(n_O\pi^*)$ state (**9**) arising from excitation of the oxygen lone pair electron to the carbonylic antibonding orbital.

To have an insight into correlation among the $^1(\pi\pi^*L_a)_{min}$, $^1(n_N\pi^*)_{min}$, and $^1(n_O\pi^*)_{min}$ structures in photophysics, we have investigated the conical-intersection geometries of $^1(\pi\pi^*L_a/ n_N\pi^*)_{CI}$, $^1(\pi\pi^*L_a/n_O\pi^*)_{CI}$, and $^1(n_N\pi^*/n_O\pi^*)_{CI}$. First, we com-

puted the adiabatic potential energy profiles of the $^1(\pi\pi^*L_a)$ and $^1(n_N\pi^*)$ states along the LIIC reaction path, connecting their minimum-energy geometries at the CASSCF level. As Figure 3 displays, the $^1(\pi\pi^* L_a/n_N\pi^*)$ conical intersection exists. Note that the formation of the $^1(\pi\pi^*L_a/n_N\pi^*)$ conical intersection is a facile process from the Frank–Condon (FC) region on the $^1(n_N\pi^*)$ state potential energy surface. The optimized geometry of $^1(\pi\pi^*L_a/n_N\pi^*)_{CI}$ is depicted in Figure 2 (**10**) and it has a planar structure similar to the $^1(\pi\pi^*L_a)_{min}$. Accordingly, we can expect that the molecule at the optimized geometry of $^1(\pi\pi^*L_a/ n_N\pi^*)_{CI}$ prefers to relax to the $^1(\pi\pi^*L_a)_{min}$ rather than the ^{1}-$(n_N\pi^*)_{min}$ structure. As Figure 4 shows, the internal conversion from the $^1(\pi\pi^*L_a)_{min}$ to the $^1(n_N\pi^*)_{min}$ structure has a barrier

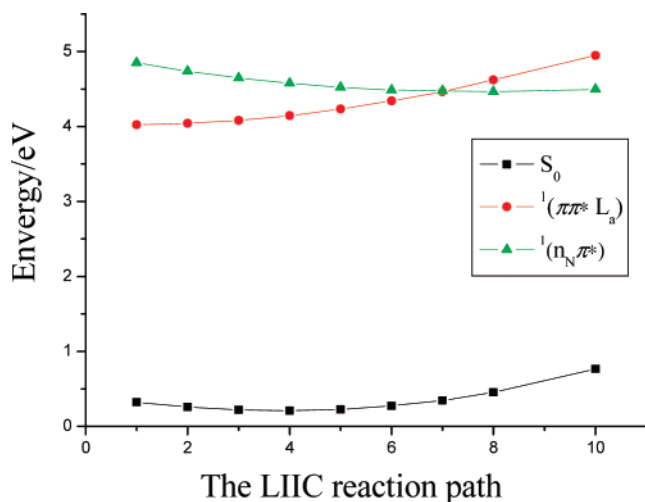Singlet Excited State of Pterin and Its Deactivation Pathway

J. Phys. Chem. A, Vol. 111, No. 38, 2007 **9259**

Figure 3. 3. CASSCF energy profiles along the LIIC reaction path from $^1(\pi\pi^*L_a)_{min}$ to $^1(n_N\pi^*)_{min}$ by the two-root state averaged CAS-(12, 9) calculation.

of 6.8 kcal/mol via the $^1(\pi\pi^*L_a/n_N\pi^*)$ conical intersection at the CASPT2 level.

The $^1(n_O\pi^*)$ state is the third excited-state at the FC ground-state geometry as mentioned in previous section. Thus, the conical intersections $^1(\pi\pi^*L_a/n_O\pi^*)_{CI}$ and $^1(n_N\pi^*/n_O\pi^*)_{CI}$ probably exist on the $^1(n_O\pi^*)$ state energy profile from the FC structure to its equilibrium state $^1(n_O\pi^*)_{min}$. The optimized geometries of $^1(\pi\pi^*L_a/n_O\pi^*)_{CI}$ and $^1(n_N\pi^*/n_O\pi^*)_{CI}$ have been given in Figure 2. As shown in Figure 2, the structures of both $^1(\pi\pi^*L_a/n_O\pi^*)_{CI}$ (**11**) and $^1(n_N\pi^*/n_O\pi^*)_{CI}$ (**12**) are nearly planar and lie at high energy levels of 113.5 and 100.7 kcal/mol, respectively.

Figure 4 summarizes the possible photophysical processes of the excited acidic form of PT from the FC geometry to their local minima $^1(\pi\pi^*L_a)_{min}$, $^1(n_N\pi^*)_{min}$, and $^1(n_O\pi^*)_{min}$ on the potential energy surfaces of low-lying excited states. In consideration of energy and absorption allowance, the acidic form of PT molecule basically was excited to the $^1(\pi\pi^*L_a)$ state under 350 nm light. The $^1(n_N\pi^*)$ state lying near the $^1(\pi\pi^*L_a)$ state at the FC structure is difficult to directly populate by electronic promotion because of the small oscillator strength. However, the $^1(n_N\pi^*)$ state is thermodynamically accessible from $^1(\pi\pi^*L_a)$ via $^1(\pi\pi^*L_a/n_N\pi^*)_{CI}$, which is lower in energy than the $^1(\pi\pi^*L_a)$ FC structure. On the contrary, two conical intersections on the potential energy surface of the $^1(n_O\pi^*)$ state, $^1(\pi\pi^*L_a/n_O\pi^*)_{CI}$ and $^1(n_N\pi^*/n_O\pi^*)_{CI}$, lie at the higher energy levels, and the high-energy $^1(n_O\pi^*)$ state with a quite small oscillator strength may not participate in the photophysical and photochemical processes at 350 nm. Hence, only the $^1(n_N\pi^*)$ and $^1(\pi\pi^*L_a)$ states are responsible for the observed fluorescence emissions experimentally. The CASPT2-predicted fluorescence spectra from $^1(\pi\pi^*L_a)$ and $^1(n_N\pi^*)$ at their minimum-energy geometries are centered at 3.14 eV (τ_{rad} = 2.7ns) and 3.36 eV (τ_{rad} = 0.3ns) in the gas phase, respectively. Because the $^1(n_N\pi^*)$ state is blue-shifted in aqueous solution, whereas the $^1(\pi\pi^*L_a)$ state with strong adsorption is red-shifted, the $^1(\pi\pi^*L_a)$ state should be mainly responsible for the experimental emission band centered at 439 nm (2.82 eV, τ_{rad} = 22 ns) in aqueous solution under irradiation of 350 nm light.

Basic Form of PT. We have successfully located the equilibrium geometries of the $^1(\pi\pi^*L_a)$ and $^1(n_N\pi^*)$ states of the basic form of PT by the CASSCF method, and at the CASPT2 level they are S_1 and S_2, respectively. As Figure 2b shows, the

$^1(\pi\pi^*L_a)_{min}$ state (**15**) has almost a planar structure with a pyramidal amino group. Just as the situation for the acidic form, the structural change in the $^1(\pi\pi^*L_a)_{min}$ state of the basic form mainly focus on the bond lengths with respect to the ground state.

The geometry optimization of the $^1(n_N\pi^*)_{min}$ state (**16**) was performed within the C_s symmetry at first, in order to avoid intrusion of other states. Although the located structure was allowed to fully relax in subsequent reoptimization, it still maintains a planar structure. In the $^1(n_N\pi^*)_{min}$ state of the basic form, because one lone-pair electron of N_6 in the molecular plane is excited to the vertical π^* orbital, the bond angle of $A(C_1N_6C_5)$ is enlarged by $\sim11°$. In calculation, we noticed that the relative energy of $^1(n_N\pi^*)_{min}$ and $^1(\pi\pi^*L_a)$ depends on the methodology. At the CASSCF level, the $^1(n_N\pi^*)_{min}$ state is lower in energy, whereas it switches with the $^1(\pi\pi^*L_a)$ state at the CASPT2 level. Their conical intersection $^1(\pi\pi^*L_a/n_N\pi^*)_{CI}$ (**17**) was found by CASSCF.

To understand the relaxation mechanisms of the excited PT, we have given the relative energy profiles of the $^1(\pi\pi^*L_a)$ and $^1(n_N\pi^*)$ states in Figure 5. It is evident that the $^1(n_N\pi^*)$ state with a small oscillator strength easily decays to the low-energy $^1(\pi\pi^*L_a)$ state via the conical intersection $^1(\pi\pi^*L_a/n_N\pi^*)_{CI}$. The CASPT2-predicted fluorescence maximum from $^1(\pi\pi^*L_a)$ at its optimized structure is about 2.61 eV (τ_{rad} = 0.94 ns) in the gas phase, which is comparable with the observed emission band centered at 456 nm (2.72 eV, τ_{rad} = 15 ns)[23] in aqueous solution at 350 nm. An interesting experimental finding is that the fluorescence spectra of PT maintain unchanged, regardless of the excitation wavelength in the range of 230−350 nm.[23] This suggests that the $^1(\pi\pi^*L_a)$ state exclusively is responsible for the emission under high-energy irradiation, and the IC processes from high-energy excited states to the $^1(\pi\pi^*L_a)$ state should be facile in the excited PT.

3.4. Radiationless Decay Path from S_1 to the Ground State. The fluorescence intensity of PT was found to decrease as the excitation energy increases,[23] suggesting that radiationless decay channel was activated under excess energy. Previous calculations on the some DNA bases[38−44] have identified IC processes via the S_1/S_0 conical intersection (denoted as $(S_1/S_0)_{CI}$) as the dominant radiationless deactivation channel. The S_1/S_0 conical intersections are induced by out-of-plane distortions arising from the twisting of C−C or C−N bonds of the six-membered ring.

Here, the IC process for both acid and basic forms of PT was discussed. The possible barrier for the formation of $(S_1/S_0)_{CI}$ on the energy surface of S_1 for the acidic form have been investigated. We optimized the geometry of $(S_1/S_0)_{CI}$ (**13**) on the basis of a starting geometry with a twisted C_8−N_9 bond. As shown in Figure 2, the optimized $(S_1/S_0)_{CI}$ structure is remarkably nonplanar. The dihedral angles of $\delta(C_5N_7C_8N_{12})$ and $\delta(C_{10}N_9C_8N_{12})$ are 118.6° and −144.6° in the acid form, respectively. The pyramidized NH_2 group is twisted by $\sim90°$ around the C_8−N_{12} bond.

The LIIC reaction path energy profiles have been calculated from the S_1 minimum geometry $^1(\pi\pi^*L_a)_{min}$ to $(S_1/S_0)_{CI}$ at the CASPT2 level. As Figure 6 shows, the IC decay from $^1(\pi\pi^*L_a)_{min}$ to the ground state via $(S_1/S_0)_{CI}$ is unfavorable thermodynamically and there is a saddle point separating the $^1(\pi\pi^*)_{min}$ and $(S_1/S_0)_{CI}$ on the potential energy surface of S_1. The saddle point structure (**14**) with one imaginary frequency of −34 cm^{-1} has been located by CASSCF (Figure 2). The structure is similar to that of $(S_1/S_0)_{CI}$, with the pyramidized and twisted amino group, and a out-of-plane deformation of ring ($\delta(C_5N_7C_8N_{12})$ = 143.0°, $\delta(C_{10}N_9C_8N_{12})$ = −159.4°).
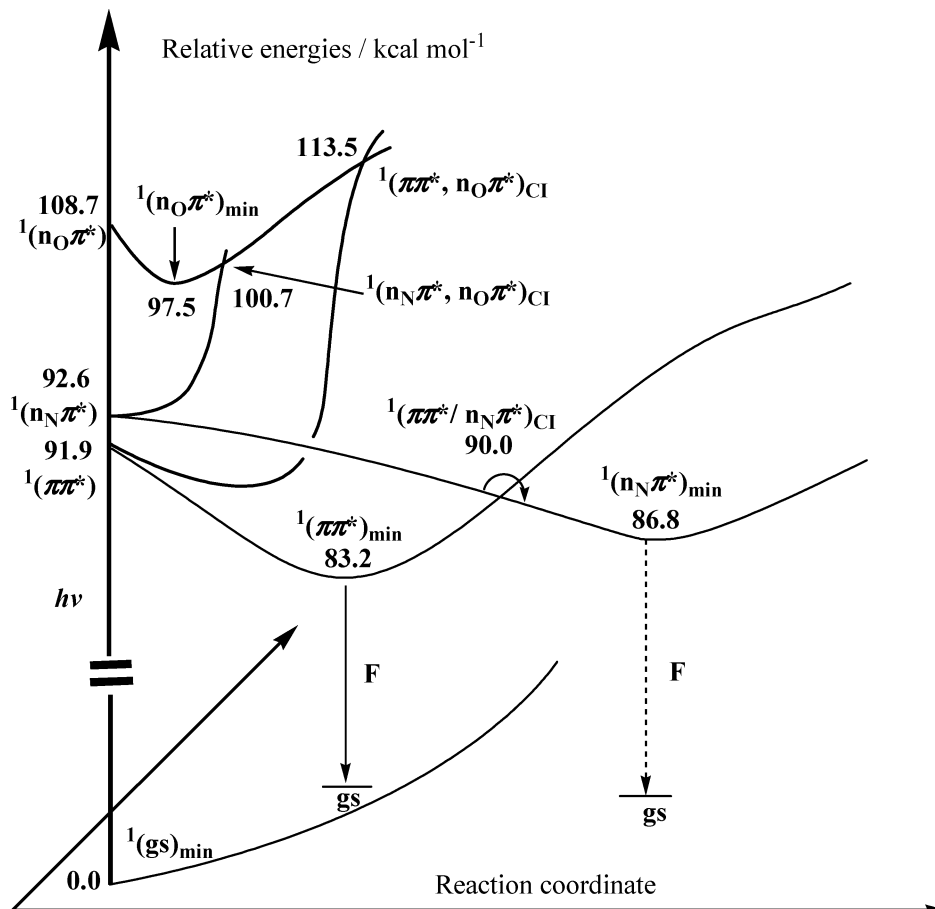
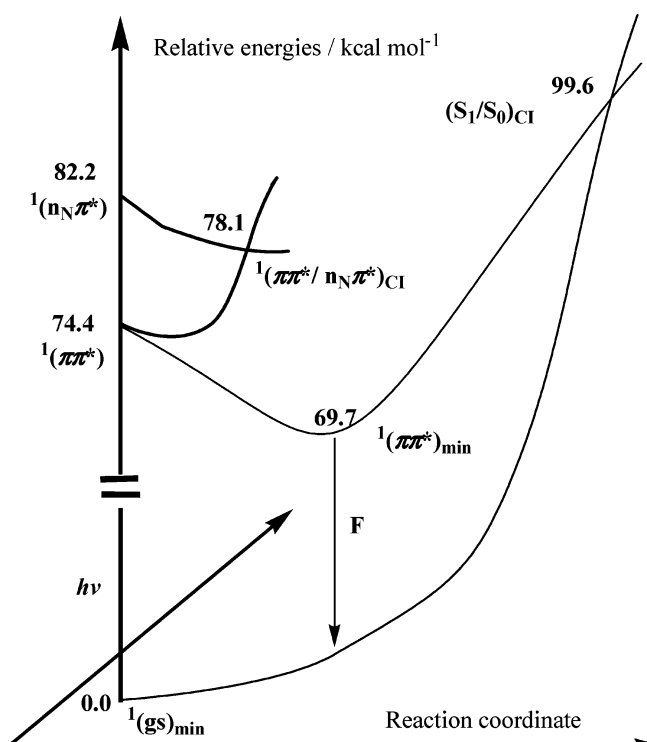**Figure 4.** 4. Relative CASPT2 energy profiles for the low-lying states of the acidic form of the excited pterin.

Figure 5. Relative CASPT2 energy profiles for the low-lying states of the basic form of the excited pterin.

Figure 6. 6. CASPT2 energy profiles along the LIIC reaction path from $^1(\pi\pi^*L_a)_{min}$ to $(S_1/S_0)_{CI}$ on the basis of the two-root state averaged CAS(12, 9) calculation.

The CASPT2 relative energies of $^1(\pi\pi^*L_a)_{min}$, the saddle point (SP), and $(S_1/S_0)_{CI}$ have been given in Figure 7. There is a barrier of 13.8 kcal/mol (0.6 eV) separating the minimum-energy
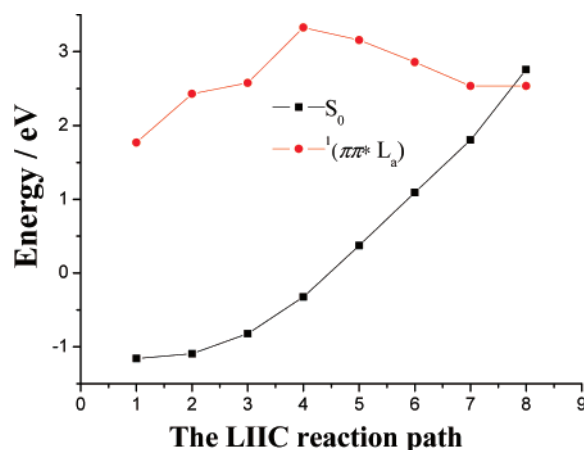
structure of the $^1(\pi\pi^*L_a)$ state from $(S_1/S_0)_{CI}$. These results can explain the experimental observations[23] that the excited PT is in favor of fluorescence emission, wherea the corresponding decay efficiency is slow ($\tau_F = 7.6$ ns) in water under the low-energy light. Once the excess energy available, the IC process via $(S_1/S_0)_{CI}$ with a out-of-plane distorted geometry will become important for fluorescence loss of PT.

Like the acid form, the conical intersection $(S_1/S_0)_{CI}$ in the basic form has a distorted structure (**18**) as shown in Figure 2. As Figure 5 shows, there is a energy gap of ~30 kcal/mol separating the minimum-energy structure of the $^1(\pi\pi^*L_a)$ state
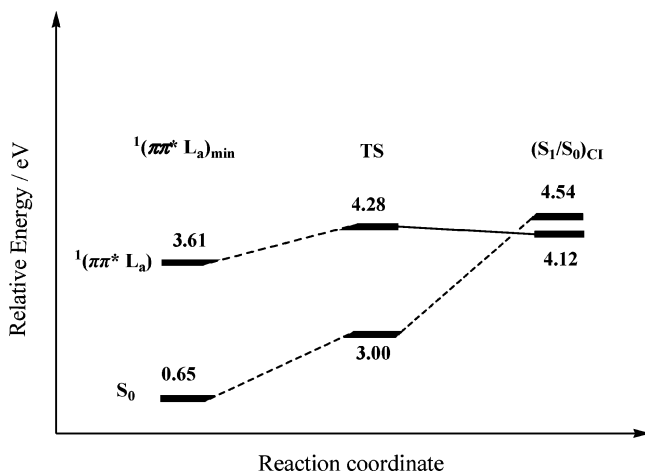
Singlet Excited State of Pterin and Its Deactivation Pathway

J. Phys. Chem. A, Vol. 111, No. 38, 2007 **9261**

Figure 7. 7. CASPT2 energy level diagram of different configurations the $^1(\pi\pi^*L_a)_{min}$, the saddle point (SP), and the $(S_1/S_0)_{CI}$ on the S_1 and S_0 potential energy surfaces of the acidic form related to the minimum energy of the ground state.

from $(S_1/S_0)_{CI}$. Therefore, the activation of such IC process requires higher energy with respect to the radiationless decay in the acid form.

If the PT molecules were elevated to higher excited-states in the FC region, e.g. $^1(\pi\pi^*L_b)$, they will rapidly decay to the more stable $^1(\pi\pi^*L_a)$ state, releasing excess energy. Subsequently, certain excited molecules at the $^1(\pi\pi^*L_a)$ state emit fluorescence and return the ground state, whereas others with excess vibrational energies may overcome the barrier and evolve to the ground state through $(S_1/S_0)_{CI}$. The latter IC process presents one plausible radiationless deactivation mechanism for the excited PT. The presence of barrier for the IC process agrees with the experimental fact that the fluorescence intensity decreases under higher-energy excitation.

4. Conclusion

For both the acidic and basic forms of PT, the most stable ground-state geometry and vertical excitation energies have been determined by DFT and ab initio calculations. The PCM model and QM/MM calculations were used to estimate the solvent effect in aqueous solution. The geometries and relative energies of local minima, conical intersections, and a saddle point on the potential energy surfaces of low-lying states have been studied by the CASSCF and CASPT2 approaches. For the acidic form of PT, most equilibrium geometries are nearly planar, whereas the optimized geometries of $(S_1/S_0)_{CI}$ and the saddle point connecting $^1(\pi\pi^*L_a)_{min}$ and $(S_1/S_0)_{CI}$ exhibit remarkable out-of-plane deformations in the ring connecting to the amino group.

The possible photophysical processes of PT have been explored. Present calculations show that the two strong absorption bands arise from dipole-allowed $\pi \rightarrow \pi^*$ transitions. The $^1(\pi\pi^*L_a)$ state is responsible for the low-energy band, and the high-energy absorption band arises from the $^1(\pi\pi^*L_b)$ state above S_2. Both $^1(\pi\pi^*L_a)$ and $^1(n_N\pi^*)$ states might be involved in the photophysics processes of the excited PT. Once the excess energy of ~0.6 eV for the acidic form and ~1.3 eV for the basic form are available, the excited PT at the $^1(\pi\pi^*L_a)_{min}$ state may decay to the ground state via the S_1/S_0 conical intersection. The IC processes with involvement of conical intersections dominate the radiationless deactivation channel for the excited PT.

References and Notes

(1) Schüttelkopf, A. W.; Hardy, L. W.; Beverley, S. M. Hunter, W. N. *J. Mol. Biol.* **2005**, *352*, 105.
(2) Heelis, P.; Kim, S. T.; Okamura, T.; Sancar, A. *J. Photochem. Photobiol., B* **1993**, *17*, 219.
(3) Johnson, J. L.; Hamm-Alvarez, S.; Payne, G.; Sancar, G. B.; Rajagopalan, K. V.; Sancar, A. *Proc. Natl. Acad. Sci. U.S.A.* **1988**, *85*, 2046.
(4) Hearst, J. E. *Science* **1995**, *268*, 1858.
(5) Nichol, C. A.; Smith, G. K.; Duch, D. S. *Annu. Rev. Biochem.* **1985**, *54*, 729.
(6) Hevel, J. M.; Marletta, M. A. *Biochemistry* **1992**, *31*, 7160.
(7) Ito, K.; Kawanishi, S. *Biochemistry* **1997**, *36*, 1774.
(8) Lorente, C.; Thomas, A. H.; Villata, L. S.; Hozbor, D.; Lagares, A.; Capparelli, A. L. *Pteridines* **2000**, *11*, 100.
(9) Pfleiderer, W. Natural pteridiness: a chemical hobby. In *Chemistry and Biology of Pteridines and Folates*; Ayling, J. E., Nair, M. G., Baugh, C. M., Eds.; Plenum Press: New York, 1993; pp 1−16.
(10) Tiemeier, H.; Fekkes, D.; Hofman, A.; van Tuijl, R. H.; Kiliaan, A. J.; Breteler, M. M. B. *Psychiatry Res.* **2006**, *145*, 199.
(11) Patterson, E. L.; von Saltza, M. H.; Stockstad, E. L. R. *J. Am. Chem. Soc.* **1956**, *78*, 5871.
(12) Fuller, R. C.; Kidder, G. W.; Nugent, N. A.; Dewey, V. C.; Rigopoulos, N. *Photochem. Photobiol.* **1971**, *14*, 359.
(13) Baur, R.; Kappel, M.; Mengel, R.; Pfleiderer, W. Photochemistry of pteridines. In *Chemistry and Biology of Pteridines*; Kisliuk, R. L., Brown, G. M., Eds.; Elsevier/North-Holland: New York, 1979; pp 13−18.
(14) Hawkins, M. E.; Pfleiderer, W.; Mazumder, A.; Pommier, Y. G.; Balis, F. M. *Nucleic Acids Res.* **1995**, *23*, 2872.
(15) Hawkins, M. E.; Pfleiderer, W.; Balis, F. M.; Porter, D.; Knutson, J. R. *Anal. Biochem.* **1997**, *244*, 86.
(16) Hawkins, M. E.; Pfleiderer, W.; Jungmann, O.; Balis, F. M. *Anal. Biochem.* **2001**, *298*, 231.
(17) Thomas, A. H.; Suárez, G.; Cabrerizo, F. M.; Martino, R.; Capparelli, A. L. *J. Photochem. Photobiol., A* **2000**, *135*, 147.
(18) Thomas, A. H.; Suárez, G.; Cabrerizo, F. M.; Capparelli, A. L. *Helv. Chim. Acta* **2001**, *84*, 3849.
(19) Thomas, A. H.; Lorente, C.; Capparelli, A. L.; Pokhrel, M. R.; Braun, A. M.; Oliveros, E. *Photochem. Photobiol. Sci.* **2002**, *1*, 421.
(20) Thomas, A. H.; Suárez, G.; Cabrerizo, F. M.; García Einschlag, F. S.; Martino, R.; Baiocchi, C.; Pramauro, E.; Capparelli, A. L. *Helv. Chim. Acta* **2002**, *85*, 2300.
(21) Lorente, C.; Capparelli, A. L.; Thomas, A. H.; Braun, A. M.; Oliveros, E. *Photochem. Photobiol. Sci.* **2004**, *3*, 167.
(22) Cabrerizo, F. M.; Petroselli, G.; Lorente, C.; Capparelli, A. L.; Thomas, A. H.; Braun, A. M.; Oliveros, E. *Photochem. Photobiol.* **2005**, *81*, 1234.
(23) Lorente, C.; Thhomas, A. H. *Acc. Chem. Res.* **2006**, *39* (6), 396.
(24) (a) Becke, A. D. *Phys. Rev. A* **1988**, *38*, 3098. (b) Lee, C.; Yang, W.; Parr, R. G. *Phys. Rev. B* **1988**, *37*, 85. (c) Becke, A. D. *J. Chem. Phys.* **1993**, *98*, 5648.
(25) (a) Cancès, M. T.; Mennucci, B.; Tomasi, J. *J. Chem. Phys.* **1997**, *107*, 3032. (b) Cossi, M.; Barone, V.; Mennucci, B.; Tomasi, J. *Chem. Phys. Lett.* **1998**, *286*, 253. (c) Mennucci, B.; Tomasi, J. *J. Chem. Phys.* **1997**, *106*, 5151. (d) Cossi, M.; Scalmani, G.; Rega, N.; Barone, V. *J. Chem. Phys.* **2002**, *117*, 43.
(26) Frisch, M. J.; Trucks, G. W.; Schlegel, H. B.; Scuseria, G. E.; Robb, M. A.; Cheeseman, J. R.; Montgomery, J. A., Jr.; Vreven, T.; Kudin, K. N.; Burant, J. C.; Millam, J. M.; Iyengar, S. S.; Tomasi, J.; Barone, V.; Mennucci, B.; Cossi, M.; Scalmani, G.; Rega, N.; Petersson, G. A.; Nakatsuji, H.; Hada, M.; Ehara, M.; Toyota, K.; Fukuda, R.; Hasegawa, J.; Ishida, M.; Nakajima, T.; Honda, Y.; Kitao, O.; Nakai, H.; Klene, M.; Li, X.; Knox, J. E.; Hratchian, H. P.; Cross, J. B.; Bakken, V.; Adamo, C.; Jaramillo, J.; Gomperts, R.; Stratmann, R. E.; Yazyev, O.; Austin, A. J.; Cammi, R.; Pomelli, C.; Ochterski, J. W.; Ayala, P. Y.; Morokuma, K.; Voth, G. A.; Salvador, P.; Dannenberg, J. J.; Zakrzewski, V. G.; Dapprich, S.; Daniels, A. D.; Strain, M. C.; Farkas, O.; Malick, D. K.; Rabuck, A. D.; Raghavachari, K.; Foresman, J. B.; Ortiz, J. V.; Cui, Q.; Baboul, A. G.; Clifford, S.; Cioslowski, J.; Stefanov, B. B.; Liu, G.; Liashenko, A.; Piskorz, P.; Komaromi, I.; Martin, R. L.; Fox, D. J.; Keith, T.; Al-Laham, M. A.; Peng, C. Y.; Nanayakkara, A.; Challacombe, M.; Gill, P. M. W.; Johnson, B.; Chen, W.; Wong, M. W.; Gonzalez, C.; Pople, J. A. *Gaussian 03*, revision C.02; Gaussian, Inc.: Wallingford, CT, 2004.
(27) MacKerell, A. D., Jr.; Bashford, D.; Bellott, M.; Dunbrack, R. L., Jr.; Evanseck, J. D.; Field, M. J.; Fischer, S.; Gao, J.; Guo, H.; Ha, S.;

Joseph-McCarthy, D.; Kuchnir, L.; Kuczera, K.; Lau, F. T. K.; Mattos, C.; Michnick, S.; Ngo, T.; Nguyen, D. T.; Prodhom, B.; Reiher, W. E., III; Roux, B.; Schlenkrich, M.; Smith, J. C.; Stote, R.; Straub, J.; Watanabe, M.; Wiorkiewicz-Kuczera, J.; Yin, D.; Karplus, M. *J. Phys. Chem. B* **1998**, *102*, 3586.

(28) Sherwood, P.; de Vries, A. H.; Guest, M. F.; Schreckenbach, G.; Catlow, C. R. A.; French, S. A.; Sokol, A. A.; Bromley, S. T.; Thiel, W.;Turner, A. J.; Billeter, S.; Terstegen, F.; Thiel, S.; Kendrick, J.; Rogers, S. C.; Casci, J.; Watson, M.; King, F.; Karlsen, E.; Sjovoll, M.; Fahmi, A.; Schäfer, A.; Lennartz, C. *J. Mol. Struct. (THEOCHEM)* **2003**, *632*, 1.

(29) (a) Ahlrichs, R.; Bär, M.; Häser, M.; Horn, H.; Kölmel, C. *Chem. Phys. Lett.* **1989**, *162*, 165. (b) Ahlrichs, R.; Bär, M.; Baron, H.-P.; Bauernschmitt, R.; Böcker, S.; Ehrig, M.; Eichkorn, K.; Elliot, S.; Furche, F.; Häser, M.; Horn, H.; Hättig, C.; Huber, C.; Huniar, U.; Kattanneck, M.; Köhn, A.; Kölmel, C.; Kollwitz, M.; May, K.; Ochsenfeld, C.; öhm, H.; Schäfer, A.; Schneider, U.; Treutler, O.; v. Arnim, M.; Weigend, F.; Weis, P.; Weiss, H. *TURBOMOLE 5.5*; University of Karlsruhe: Karlsruhe, Germany, 2002.

(30) (a) Stratmann, R. E.; Scuseria, G. E.; Frisch, M. J. *J. Chem. Phys.* **1998**, *109*, 8218. (b) Bauernschmitt, R.; Ahlrichs, R. *Chem. Phys. Lett.* **1996**, *256*, 454. (c) Casida, M. E.; Jamorski, C.; Casida, K. C.; Salahub, D. R. *J. Chem. Phys.* **1998**, *108*, 4439.

(31) Roos, B. O. *Adv. Chem. Phys.* **1987**, *69*, 399.

(32) Werner, H.-J.; Knowles, P. J.; Amos, R. D.; Bernhardsson, A.; Berning, A.; Celani, P.; Cooper, D. L.; Deegan, M. J. O.; Dobbyn, A. J.; Eckert, F.; Hampel, C.; Hetzer, G.; Knowles, P. J.; Korona, T.; Lindh, R.; Lloyd, A. W.; McNicholas, S. J.; Manby, F. R.; Meyer, W.; Mura, M. E.; Nicklass, A.; Palmieri, P.; Pitzer, R.; Rauhut, G.; Schütz, M.; Schumann, U.; Stoll, H.; Stone, A. J.; Tarroni, R.; Thorsteinsson, T.; Werner, H.-J. *MOLPRO*, version 2006.1.

(33) Zhanpeisov, N. U.; Leszczynski, J. *Struct. Chem.* **2001**, *12*, 121.

(34) Lim, E. C. *J. Phys. Chem*. **1986**, *90*, 6770.

(35) Platt, J. R. *J. Chem. Phys.* **1949**, *17*, 484.

(36) Shukla, M. K.; Leszczynski, J. *J. Phys. Chem. A* **2002**, *106*, 11338.

(37) Langer, H.; Doltsinis, N. L. *J. Chem. Phys.* **2003**, *118*, 5400.

(38) Chen, H.; Li, S. H. *J. Phys. Chem. A* **2005**, *109*, 8443.

(39) Blancafort, L. *J. Am. Chem. Soc.* **2006**, *128*, 210.

(40) Perun, S.; Sobolewski, A. L.; Domcke, W. *J. Am. Chem. Soc.* **2005**, *127*, 6257.

(41) Shukla, M. K.; Mishra, P. C. *Chem. Phys.* **1999**, *240*, 319.

(42) Matsika, S. *J. Phys. Chem. A* **2004**, *108*, 7584.

(43) Ismail, N.; Blancafor, L.; Olivucci, M.; Kohler, B.; Robb, M. A. *J. Am. Chem. Soc.* **2002**, *124*, 6818.

(44) Merchan, M.; Serrano-Andre, L. *J. Am. Chem. Soc.* **2003**, *125*, 8108.